



2022

Fluorescence detection of malachite green in fish based on aptamer and SYBR Green I

Follow this and additional works at: <https://www.jfda-online.com/journal>

 Part of the [Food Science Commons](#), [Medicinal Chemistry and Pharmaceutics Commons](#), [Pharmacology Commons](#), and the [Toxicology Commons](#)



This work is licensed under a [Creative Commons Attribution-Noncommercial-No Derivative Works 4.0 License](#).

Recommended Citation

Wang, Jia; Hong, Chengyi; Lin, Zhengzhong; and Huang, Zhi-Yong (2022) "Fluorescence detection of malachite green in fish based on aptamer and SYBR Green I," *Journal of Food and Drug Analysis*: Vol. 30 : Iss. 3 , Article 4.

Available at: <https://doi.org/10.38212/2224-6614.3422>

This Original Article is brought to you for free and open access by Journal of Food and Drug Analysis. It has been accepted for inclusion in Journal of Food and Drug Analysis by an authorized editor of Journal of Food and Drug Analysis.

Fluorescence detection of malachite green in fish based on aptamer and SYBR Green I

Jia Wang, Chengyi Hong, Zhengzhong Lin, Zhi-Yong Huang*

College of Ocean Food and Biological Engineering, Jimei University, Xiamen, China

Abstract

A simple fluorescence method to quantitatively monitor malachite green (MG) was introduced based on the conformation switch effect of MG-aptamer (Apt) and the fluorochrome of SYBR Green I (SGI). SGI can embed in the stem-loop structure of Apt to produce fluorescence. However, the fluorescence will be quenched when MG is introduced because of the specific binding of Apt to MG. Under the optimal conditions, the fluorescence method displayed excellent linear relationship between the fluorescence quenching efficiencies and the MG concentrations ranging from $0.02 \mu\text{mol L}^{-1}$ to $1.0 \mu\text{mol L}^{-1}$. The detection limit of the method was $0.67 \mu\text{g kg}^{-1}$ ($3\sigma/\kappa$, $n = 9$) which is lower than the limit ($1 \mu\text{g kg}^{-1}$) specified in the national standard of China (GB/T 19857–2005) and the limit ($2 \mu\text{g kg}^{-1}$) specified by the European Food Safety Authority (EFSA, 2016). Excellent recoveries between 87.1% and 106.9% tested by spiking standards were achieved with RSD less than 6.4%. The data were confirmed by the method of HPLC, and the results proved that the established fluorescence method could be used for the rapid detection of MG in fish with high accuracy and sensitivity.

Keywords: Aptamer, Conformation switch effect, Food safety, Malachite green, SYBR Green I

1. Introduction

Malachite green (MG) is a poisonous cationic triarylmethane dye which has commonly been utilized in the preparation of paper [1], leather [2], and battery manufacturing [3] and food packing [4]. The uncontrolled discharging of wastewater containing MG has been regarded as one of the main causes of MG pollution in water [5]. Meanwhile, MG has been widely used in the process of aquaculture as a fungicide, disinfectant, and parasiticide since 1933 [6]. However, MG is clearly listed as a prohibited veterinary drug by most countries [7], including the United States, Canada, and the European Union, because of its potential carcinogenic [8], genotoxic [9], teratogenic properties [10], respiratory toxicity [11], in addition to other various side effects toward humans and animals [12]. Nevertheless, MG has been illegally used due to its low cost, availability, high efficacy against hard-to-control parasites and fungal diseases, and lack of proper supervision [13].

Numerous instrumental analytical techniques, including liquid chromatography-mass spectrometry (LC-MS) [14], high-performance liquid chromatography (HPLC) [15], and enzyme linked immunosorbent assay (ELISA) [16], have been developed for the measurement of MG. However, the inherent defects of instrumental analytical techniques such as complex extraction procedures [17] and costly solid-phase extraction columns [18], and rigorous analytical conditions [19], hinder the application of these methods in the rapid detection of MG in foods. Therefore, the development of a rapid, low-cost, and sensitive method for MG detection is highly desired.

Bio-probers have been employed as tools for MG detection [20]. Aptamers (Apts), which are generally derived from DNA and RNA [21], have been widely employed in the fields of therapeutics [22], molecular imaging [23], and biosensors [24]. Apts are promising alternatives to antibodies in probes due to their remarkable molecular recognition features [25]. In particular, sensing strategies based on Apts

Received 15 June 2022; revised 3 July 2022; accepted 7 July 2022.
Available online 15 September 2022

* Corresponding author.
E-mail address: zhyhuang@jmu.edu.cn (Z.-Y. Huang).

<https://doi.org/10.38212/2224-6614.3422>

2224-6614/© 2022 Taiwan Food and Drug Administration. This is an open access article under the CC-BY-NC-ND license (<http://creativecommons.org/licenses/by-nc-nd/4.0/>).

ORIGINAL ARTICLE

have shown extraordinary advantages compared with those of natural antibodies or enzymes [26], such as small molecular size, low cost, specificity, rapid response and conformational changes upon targets/analytes binding [27,28]. In recent years, methods of MG detection using aptamers have been developed, such as colorimetric method based on Aptamer/AuNP [29], electrochemical method [30], fluorescence method based on split-type aptamer [31], etc. However, these methods generally have a narrow linear range, complex sample pretreatment, high detection limits. Most importantly, these methods usually use RNA as the recognition unit, which is expensive and easily degraded by RNases [32].

SYBR Green I (SGI) is a highly sensitive anthocyanin nucleic acid gel dye that can be used for the quantitative detection of double- or single-stranded DNA or RNA based on complementary base pairing [33]. The advantages of low background noise, high sensitivity, and simplicity make SGI promising in sensing field based on photophysical properties [34].

The MG-DNA Apt has a unique stem-loop structure with double-stranded complementary sequences at its head and tail [35]. Inspired by this feature, we proposed a novel detection strategy based on MG-DNA Apt and SGI in the present study. The fluorescence signal of the detection system can be observed when the Apt binds to SGI because of the embedding effect of SGI in the stem-loop of Apt. However, the fluorescence can be quenched when MG is introduced, which may be due to the occupation of MG in the specific recognition site of the stem-loop of Apt. By measuring the fluorescence quenching efficiency, the fluorescence method can be developed to quantitatively detect MG residues in fish samples.

2. Experimental section

2.1. Reagents

The MG-Apt sequence [35] is 5-CTCA-GATCTAACCTTG TTAAATTGAG-3', SGI, Gel Red, SYBR Gold, and ethidium bromide were purchased from Shanghai Sangon Technologies Inc. (Shanghai, China). MG, leucomalachite green (LMG), sulfadimethoxine (SDM), sulfonamide (ST), methyl orange (MB), methyl red (MR), chloramphenicol (CAP), crystal violet (CV), nitrofurazone (NU), brilliant green (BG), tetracycline hydrochloride (TCT) and formaldehyde (FM) were all purchased from Shanghai Aladdin Biochemical Technology Inc. (Shanghai, China). Hydroxylamine hydrochloride and 2-morpholineethanesulfonic acid

were purchased from Xilong Scientific Inc. (Shantou, China).

The other aptamers included in the experiment were shown in Appendix (Supplementary data).

2.2. CD spectroscopy and UV-vis characterization

The reaction of MG and Apt was characterized by CD color spectroscopy using a JASCO J-815 circular dichroism spectrometer (Light Corporation, Japan). Three 10 mL centrifuge tubes were used and marked as a, b and c, respectively. Each of 2.5 mL $1 \mu\text{mol L}^{-1}$ Apt solutions was added to tubes. Then, 1 mL of MG solutions with the concentrations of $0.5 \mu\text{mol L}^{-1}$ and $2 \mu\text{mol L}^{-1}$ was added to tube b and c, respectively. Ultrapure water was used to adjust a, b, and c to obtain 5 mL for each tube. After incubating at room temperature for 30 min, 1 mL of the reaction solution was pipetted and added to the circular dichroism cuvette (optical path of 10 mm). CD spectra of the reaction system were recorded in the range of 220–320 nm at a scan speed of 100 nm min^{-1} . The data collected were the average of three scans.

UV-vis spectra were measured using a Lambda 265 UV spectrophotometer (Perkin Elmer, America). Four centrifuge tubes (2 mL) were used and labeled as a, b, c, and d. Then, 100 μL of $1 \mu\text{mol L}^{-1}$ Apt solutions (prepared with ultrapure water) was added to each tube. And each of 100 μL of MG with different concentrations (0.5 , 2.5 , and $5 \mu\text{mol L}^{-1}$) was added to tube b, c and d, respectively. The total volume of each tube was adjusted to 500 μL with ultrapure water. After incubation at room temperature for 30 min, 200 μL of the solutions was taken for UV-vis spectral scanning from 220 nm to 340 nm.

2.3. Fluorescent detection of MG

Fluorescent analysis was performed under the following procedure. At room temperature, 100 μL of $1 \mu\text{mol L}^{-1}$ Apt solutions (diluted with ultrapure water) was mixed with 100 μL of MG standard solutions or sample solutions. After vortex oscillation at room temperature for 20 min, 30 μL of $10 \times$ SGI (diluted to 1000 times with ultrapure water) was added. Then, 270 μL of ultrapure water was added to obtain 500 μL of mixture. After continually incubating for 10 min, the solutions were transferred to cuvette for fluorescence measurement with the excitation wavelength of 495 nm and the emission wavelength of 530 nm. The fluorescence quenching efficiency was evaluated by $(F_0 - F)/F_0$, where F_0 represents the fluorescence intensity in the absence

of MG, and F represents the fluorescence intensity in the presence of MG. At the same time, the mixed solutions were photographed using a smartphone under UV lamp. Three replicates were set for each sample.

2.4. Selectivity and anti-interference test

The structural analogs of MG, LMG, CV, BG, MR and MB were used to test the selectivity of the method. In addition, several common veterinary drugs, such as NU, SDM, ST, CAP, and FM, were utilized for selective testing. The anti-interference ability of the detection method was also determined by measuring the binary mixtures including MG + LMG, MG + CV, MG + BG, MG + MR, MG + MB, MG + SDM, MG + ST, MG + NU, MG + TCT, MG + CAP, and MG + FM. The $(F_0 - F)/F_0$ values were measured for comparative analysis. The final concentration of MG in the experiments was set as $0.2 \mu\text{mol L}^{-1}$, and all of the concentrations of interfering substances were set as $2 \mu\text{mol L}^{-1}$. Each group of experiments was set at three replicates.

2.5. Real sample analysis

Fish samples in the experiment came from the Jiageng Farmers Market in Xiamen City, China. Sea water was taken from local aquaculture farms. Fish and shrimp samples were treated using the previous processing method [29] with slight modifications. Specifically, the live fish were first slaughtered, and the head and tail were removed. About 5 g of meat cut from back using a ceramic knife was accurately weighed into a 50 mL centrifuge tube, and 2.5 mL of 1 mol L^{-1} ammonium acetate buffer, 0.5 mL of 0.25 g mL^{-1} hydroxylamine hydrochloride solution, 50 μL of 1 mol L^{-1} p-toluenesulfonic acid solution and 7.5 mL acetonitrile were added. The resultants were then transferred to an analytical grinder (IKA, Germany) for crushing and homogenization. After homogenizing for 5 min, the slurries were transferred to a centrifuge tube. Then, the mixtures were shaken for 30 min, and the samples were centrifuged at 4°C for 5 min (5000 rpm). The supernatants were transferred to 200 mL pear-shaped separatory funnels, and the precipitates were extracted again using 25 mL of acetonitrile. Then, the combined extracting solutions were further extracted twice using dichloromethane each of 25 mL. The lower layer solutions were collected and dried with nitrogen atmosphere at 50°C . The residues were dissolved in 2 mL of ultrapure water and filtered through a $0.22 \mu\text{m}$ filter. Each of 190 μL of the filtrate

was collected and mixed with 10 μL of MG standard solutions for recovery tests. Sea water samples were filtered through a $0.22 \mu\text{m}$ filter and mixed with MG standards for recovery tests.

2.6. HPLC detection conditions

The experimental conditions of HPLC were as follows: Eclipse Plus C_{18} chromatographic column, 50 mmol L^{-1} of ammonium acetate buffer (pH 4.5) as mobile phase A and acetonitrile as mobile phase B ($V_A:V_B = 4:6$), 20 μL of injection volume, 0.5 mL min^{-1} of flow rate. The separation was performed at 25°C , and the detection wavelength was 618 nm.

3. Results and discussion

3.1. Design strategies

Fig. 1 shows that the detection method is designed according to the inherent stem-loop structure and structure conversion effect of the Apt. Given that SGI has a super-strong affinity for double-stranded DNA molecules, it can intercalate into the stem-loop region of MG-Apt, resulting in a strong fluorescent signal [36]. However, when the target MG exists, MG specifically binds to Apt and occupies its stem-loop recognition region, which causes the structure of Apt to undergo a distorted transition [37]. The distorted conformation and steric hindrance effect prevent SGI from entering the groove of Apt, leading to the fluorescent quenching. Therefore, MG can be quantitatively detected according to the decreases of fluorescence signals.

The fluorescence spectra of Apt/SGI, Apt/MG/SGI, SGI, and SGI/MG were scanned at 510–700 nm under the excitation wavelength of 495 nm to verify the feasibility of the detection method. As shown by the line c in Fig. 2, SGI alone has nearly no fluorescence emission when Apt is absent in the solution. However, SGI can quickly embed into the double-stranded structure and groove of Apt after mixing with Apt, and an obvious fluorescence emission peak at 530 nm is observed as shown in line a, which implies that SGI is bound to Apt. As shown in line b, after adding MG the fluorescence decreases sharply, which may be due to the specific binding effect of MG to Apt. The occupation of MG in the recognition site of Apt leads to the conformational change of Apt, preventing the fluorescent staining of SGI to Apt. Therefore, the fluorescent method is proved to be feasible for MG detection.

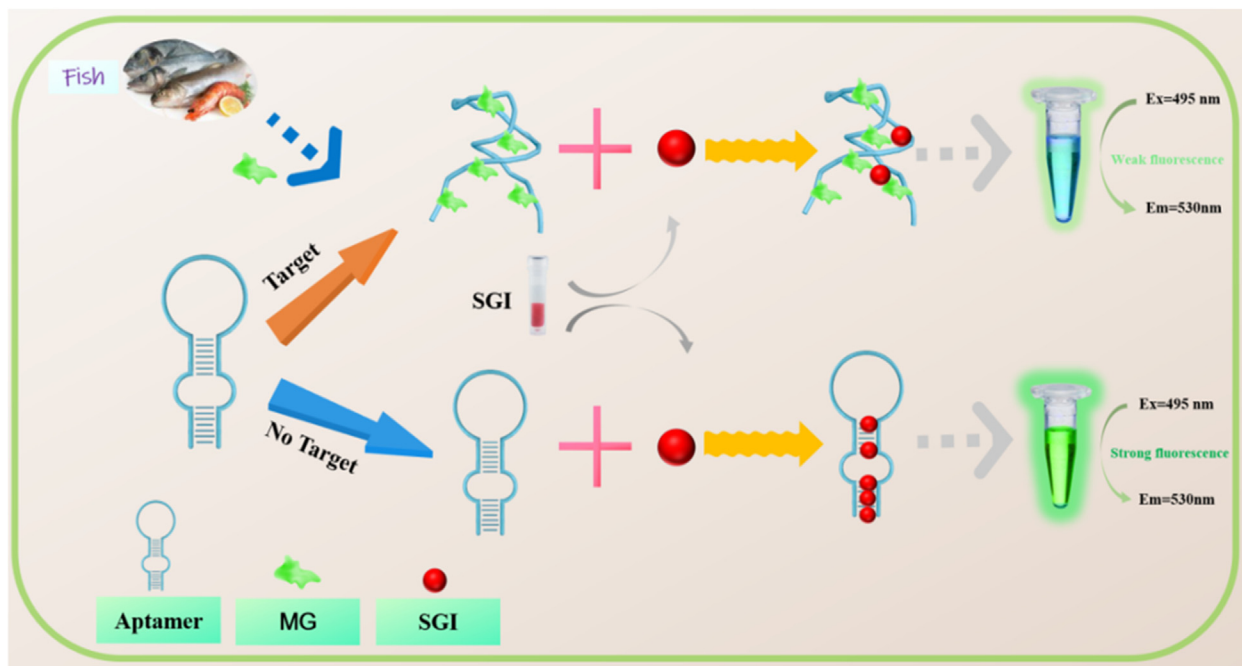


Fig. 1. Scheme of the structure-switching fluorescence method for MG detection.

3.2. Characterization of CD spectroscopy and UV-vis

Circular dichroism (CD) is an important tool for evaluating the conformational changes of Apts. As shown the line a in Fig. 3(A), in the absence of MG the Apt solution has an obvious negative peak at 245 nm and a positive peak at 275 nm, which is the typical DNA double-helix structure due to the member of right-handed B-DNA family [38]. After adding of MG, the peak positions of Apt did not change significantly, but the peak high changed.

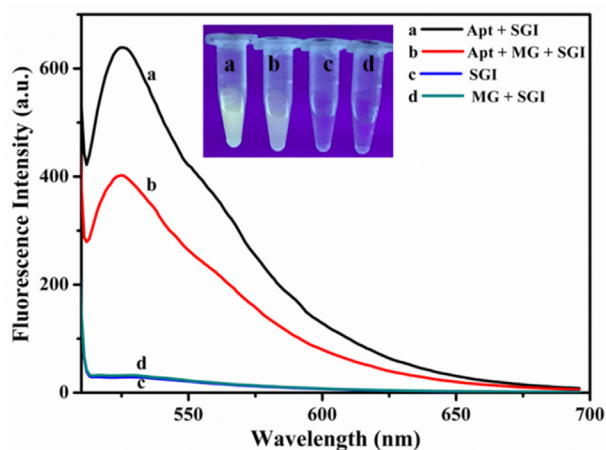


Fig. 2. Fluorescence spectra of SGI in different systems. (Concentrations of SGI: 0.6×10^{-6} mol L⁻¹, Aptamer: $0.3 \mu\text{mol L}^{-1}$, MG: $0.2 \mu\text{mol L}^{-1}$, inset: the photofluorography under 365 nm UV light).

Both of the positive peak and the negative peak were enhanced, which might be due to the binding effect of MG and Apt and results in the distortion of double-helix structure of Apt. Therefore, the fluorescence staining of SGI in the mixture of MG and Apt disappeared. The UV-vis spectra in Fig. 3(B) show that the Apt solution alone has an obvious absorption peak at 260 nm, but the absorption peak decreases with the increases in MG concentrations. The result may be due to the disordered stacking effects of Apt bases after the addition of MG [39]. The results further confirm that the fluorescence staining of SGI in the mixture of MG and Apt is unable to be carried on.

3.3. Apt specificity

As shown in Fig. 4A, the coloring of SGI dye occurs with different Apts to generate fluorescent signals. The fluorescence staining of SGI with CAP-Apt, OTA-Apt and SDM-Apt may be due to the G-quadruplex structures of these Apts. However, all the $(F_0 - F)/F_0$ values are low except for MG-Apt, which can be interpreted that the specific recognition of MG to MG-Apt. In addition, MG tailor-made Apts with different lengths of bases, including 26 bases of Apt, 13 bases (Prope-1), 19 bases (Prope-2), and 33 bases (Prope-3) were investigated in terms of $(F_0 - F)/F_0$ values. As shown in Fig. 4B, the truncated or lengthened MG tailor-made Apts result in obvious lower of fluorescence

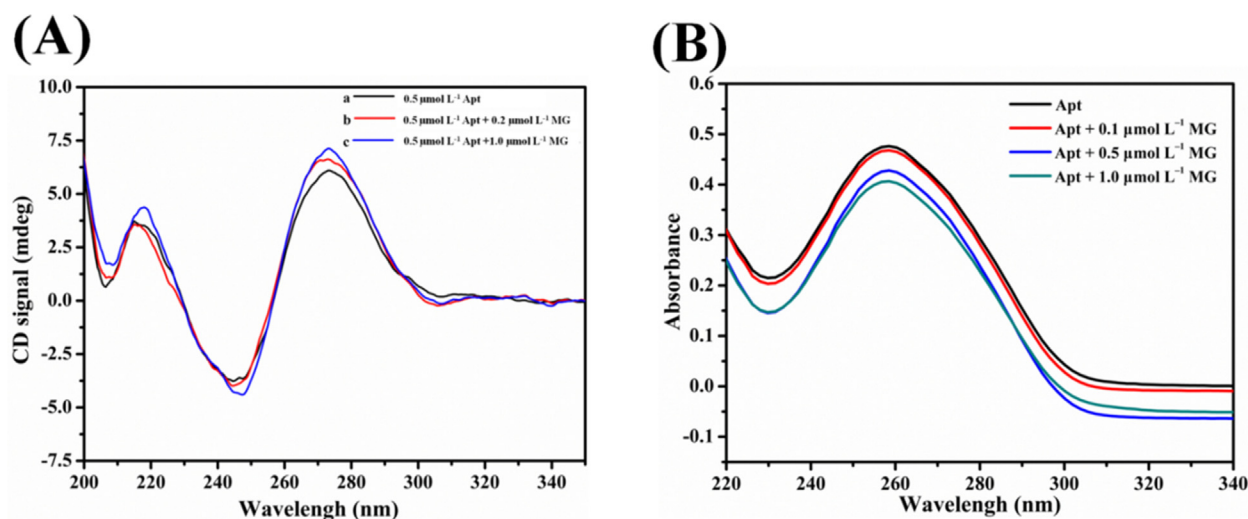


Fig. 3. (A) Circular dichroism spectra and (B) UV-vis spectra of Apt mixed with MG.

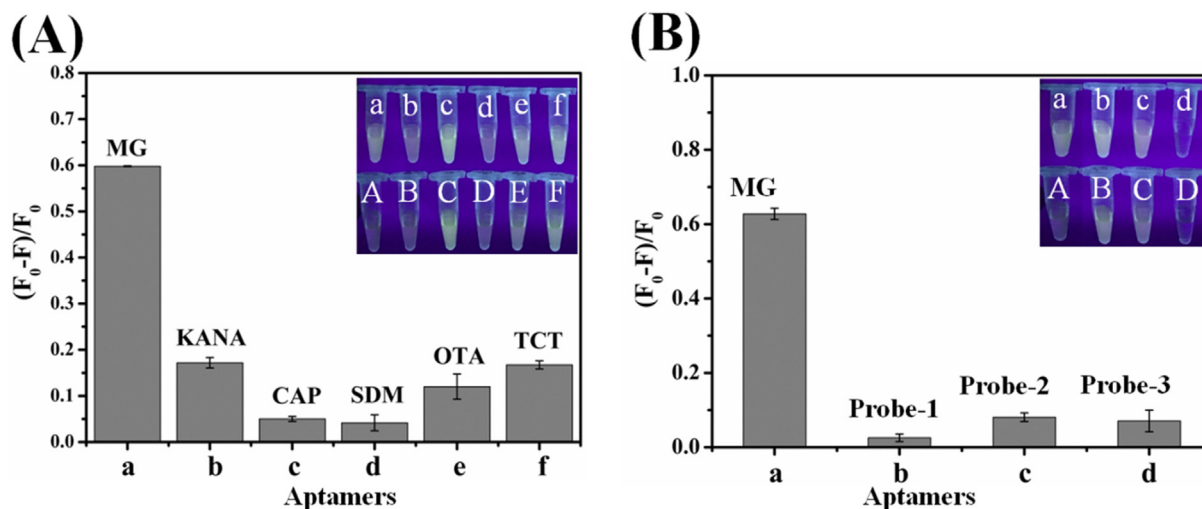


Fig. 4. Comparison of the fluorescence quenching efficiency $(F_0 - F)/F_0$ of different aptamers ($0.3 \mu\text{mol L}^{-1}$) with MG ($0.2 \mu\text{mol L}^{-1}$). Different kinds of aptamers (A) and truncated or lengthened MG tailor-made Apts (B). (error bars represent the standard deviations of three replicates. Insets: lowercases represent the photofluorography in the absence of MG, while capital letters represent the presence of MG).

quenching efficiencies compared with that of MG-Apt with 26 bases. The length of MG-Apt may play an important role on the binding ability between the aptamer and SGI. In addition to the interaction within the groove of MG-Apts, the intercalation between base pairs and the stabilization of the electrostatic SGI/DNA complex contributes to the affinity of SGI to DNA [34]. Therefore, the MG-Apt with 26 bases was used throughout the experiment considering the strong fluorescence intensity and the high fluorescence quenching efficiency.

3.4. Optimization of experimental conditions

Several parameters, including buffer and pH, Apt concentration, SGI concentration, and reaction time,

were optimized based on the fluorescence and the $(F_0 - F)/F_0$ values. The concentration of MG was set as $1 \mu\text{mol L}^{-1}$ in all the optimization.

3.4.1. Choice of nucleic acid dyes

Many dyes can specifically bind to double-stranded DNA. As shown in Fig. S1, SGI has the highest $(F_0 - F)/F_0$ value compared with those of Gel red, EB and SYBR gold. The combination of Gel Red and Apt generates strong fluorescence (inset tube B), but the $(F_0 - F)/F_0$ value is the smallest (inset tube b). It has been found that the binding ability of Gel red to dsDNA was about two times stronger compared with the binding to ssDNA. In addition, about five times stronger of binding ability of Gel red to ssDNA can be achieved compared with that

of SGI to ssDNA [40]. The strong fluorescence from tube B might be interpreted that Gel Red solidly inserted into the double-stranded and the groove of Apt, which prevented MG from the specific binding site in Apt and resulted in low fluorescence quenching efficiency. High quenching efficiencies were also obtained with EB and SYBR Gold, but their fluorescence intensities were low (inset tube C and D) which may seriously decrease the analytical sensitivity. In addition, EB is a highly toxic nucleic acid dye [41], and SYBR Gold is unstable and expensive. Hence, SGI was finally employed as the nucleic acid dye throughout the experiment.

3.4.2. Buffer selection

Appropriate reaction medium may be an important condition for biochemical reactions because of the ionization equilibrium and affinity capacity of molecular [42]. As shown in Fig. S2 (A), highest fluorescence intensity is obtained in ultrapure water (ddwater), while HEPES buffer presents the lowest which may be due to the electrostatic interaction between HEPES and SGI. In addition, highest $(F_0-F)/F_0$ value is observed in ultrapure water as shown in Fig. S2 (B). Therefore, ddwater was selected as the reaction medium in the detection system.

3.4.3. Buffer pH

As shown in Fig. S3(A), pH value ranging from 6.3 to 7.5 has little effect on the fluorescence quenching efficiency, but relative high $(F_0-F)/F_0$ values are observed for pH above 6.9. The result in Fig. S3(B) shows that the fluorescence intensity decreases slightly with the increase of pH value. In order to obtain high detection sensitivity, the optimum pH was chosen as 6.9.

3.4.4. Apt concentration

As shown in Fig. S4(B), the fluorescence intensities of detection system increase with the rises of Apt concentrations. The reason may be that the sufficient Apt can provide the plenty binding sites for the intercalation of SGI and MG. When the Apt concentration was $0.2 \mu\text{mol L}^{-1}$, the $(F_0-F)/F_0$ value reaches the maximum as shown in Fig. S4(A). However, continuously increasing Apt concentration could still increase the fluorescence intensities, but the $(F_0-F)/F_0$ value decreased obviously. Therefore, the concentration of Apt was set as $0.2 \mu\text{mol L}^{-1}$.

3.4.5. SGI concentration

SGI concentration is an important parameter affecting the sensitivity of the fluorescence method

as shown in Fig. S5. The fluorescence intensities significantly increased with the increases of SGI concentrations until the growth rate slowed down after $0.6 \times$. And the $(F_0-F)/F_0$ value reached the maximum when the SGI concentration was above $0.4 \times$. In order to ensure the adequate concentration of SGI, its dilution ratio was set as $0.6 \times$ (diluted to 60000 times with ultrapure water).

3.4.6. Reaction time

As shown in Fig. S6, the $(F_0-F)/F_0$ values increase with the binding time of MG and Apt until 20 min. Therefore, the binding time of MG and Apt was set as 20 min.

As shown in Fig. S7, the $(F_0-F)/F_0$ value reaches an equilibrium stage after the incubation time of SGI in the detection system is 600 s. Therefore, 600 s (10 min) was chosen as the incubation time after SGI was added in the detection solution.

3.5. Performance of the MG detection

Under the optimal conditions, MG standard solutions and samples were analyzed with the constructed fluorescent method. As shown in Fig. 5(A), the fluorescence intensities at 530 nm gradually decreases with the increases of MG concentrations in the range of $0.02 \mu\text{mol L}^{-1}$ – $1.2 \mu\text{mol L}^{-1}$. Fig. 5 (B) shows that the concentrations of MG ranging from $0.02 \mu\text{mol L}^{-1}$ to $0.4 \mu\text{mol L}^{-1}$ and the $(F_0-F)/F_0$ values have an excellent linear relationship with a linear equation of $Y = 1.756X + 0.09$ ($R^2 = 0.992$), and another linear relationship of $Y = 0.226X + 0.69$ ($R^2 = 0.928$) is fit for MG concentrations ranging from $0.4 \mu\text{mol L}^{-1}$ to $1.2 \mu\text{mol L}^{-1}$. The detection limit (LOD, $3\alpha/\kappa$, $n = 9$) is $0.004 \mu\text{mol L}^{-1}$ tested with the standard blank solutions. In order to test the LOD of the detection method, nine blank samples were used and the LOD of the fluorescence method is $0.67 \mu\text{g kg}^{-1}$ ($3\alpha/\kappa$, $n = 9$). The method's LOD is lower than the limit ($1 \mu\text{g kg}^{-1}$) specified in the national standard of China (GB/T 19857–2005) and the limit ($2 \mu\text{g kg}^{-1}$) specified by the European Food Safety Authority (EFSA, 2016).

Table 1 compared the present method with the previous methods for MG detection. The LOD of the present method is not as good as those of LC-MS [43], HPLC [44], ELISA [45] and SERS [46]. However, the present method is simple and low cost, time-saving, and does not require expensive instrument. Compared with the spectrophotometric method [47], the present method not only has a lower LOD value but also overcomes the disadvantages such as the requirement of extraction columns for sample preparation. The present LOD is similar to that of

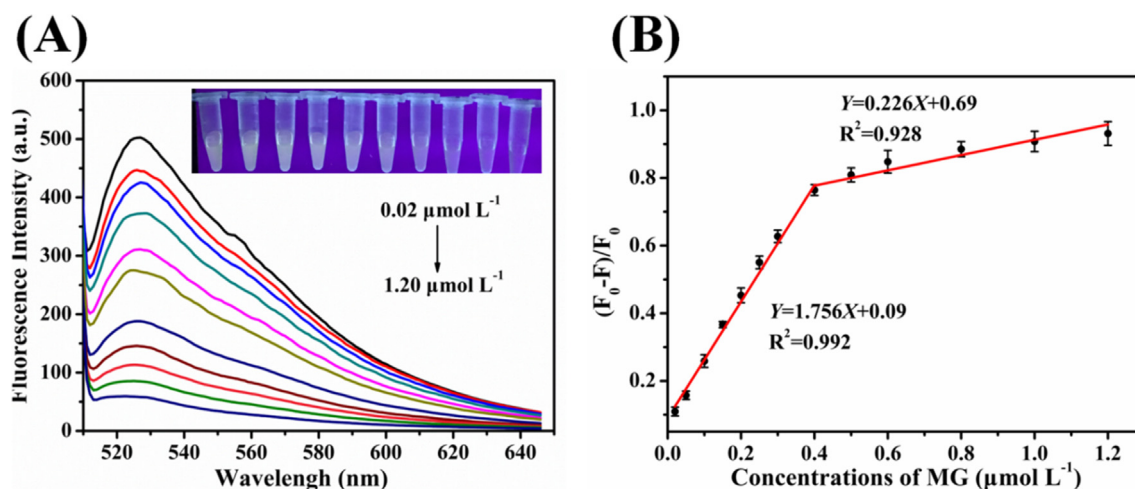


Fig. 5. (A) Fluorescence spectra of detection solutions containing different concentrations of MG ($0.02\text{--}1.2\ \mu\text{mol L}^{-1}$), and (B) linear relationship of MG concentrations and fluorescence quenching efficiencies. (Inset: the photofluorography under 365 nm UV light).

Table 1. Comparison of analytical parameters of different methods in MG detection.

Methods	Linear ranges ($\mu\text{g L}^{-1}$)	LOD ($\mu\text{g L}^{-1}$)	Recovery (%)	Samples	References
LC-MS	0.4–3.0	$0.13\ \mu\text{g kg}^{-1}$	103–110	Fish	[43]
HPLC	0.3–15.0	$0.15\ \mu\text{g kg}^{-1}$	71.8–96.8	Fish	[44]
ELISA	50.0–6250.0	0.37	76.2–82.9	Fish	[45]
Spectrophotometric	60–600	2.2	90.0–115.0	Water	[47]
	1.0–1000.0	$1\ \mu\text{g kg}^{-1}$	96.6–111.5	Fish	[46]
Electrochemical	3.6–363.5	1.22	98.5–102.2	Fish	[48]
	6.6–23.2	6.5	Not mentioned	Tea	[49]
Fluorescence	69.0–7270	109.1	96.4–106.0	Fish	[50]
	3.6–181.7	0.65	88.0–135.0	Water	[51]
Colorimetry	7.3–109.5	5.82	96–104.8	Fish	[29]
	7.3–145.4	1.46	87.1–106.9	Fish/Water	This work
	($0.02\text{--}0.4\ \mu\text{mol L}^{-1}$)	($0.61\ \mu\text{g kg}^{-1}$)			

the electrochemical method [48], but the electrochemistry requires complex nanomaterials for electrode preparation. Fluorescence and colorimetric methods based on carbon dot, gold nanoclusters and AuNPs have been developed for MG detection [49–51]. But MG-RNA Apts or antibodies were often used as recognition elements, which might greatly increase the detection cost, and were unstable for RNA Apt due to the RNase [52].

3.6. Specificity and selectivity

In order to investigate the selectivity and anti-interference of the method, several drugs including structural analogs of MG, LMG, BG, and CV, industrial dyes such as MR and MB, and some antibacterial drugs such as CAP, SDM, ST, TCT, and FM, which may be used in aquaculture were tested [53,54]. Based on the fluorescence quenching efficiencies, the drugs were tested for assessing the selectivity of MG detection. In addition, several binary mixtures containing MG were used to

investigate the anti-interference abilities of the fluorescence method. As shown in Fig. 6, compared with these testing drugs only MG shows the excellent $(F_0-F)/F_0$ value, which may be due to the specific binding of MG to Apt. LMG shows a little interference which may be due to the similar structure to MG, but there is no interference for MG detection checked by paired t -test ($p > 0.05$).

3.7. Real sample detection

In order to verify the practicability of the fluorescence method, sturgeon, prawn, and seawater were used for MG detection by spiked recovery experiments, and were verified by HPLC method. Data in Table 2 show that the recoveries of 87.1%–106.9% (RSD 3.5%–6.4%) by the fluorescence method are similar to those (recovery 88.5%–103.2%, RSD 3.2%–8.1%) of HPLC method. There is no significant difference ($p > 0.05$) between the data collected from the two methods, indicating that the established fluorescence method can be used to

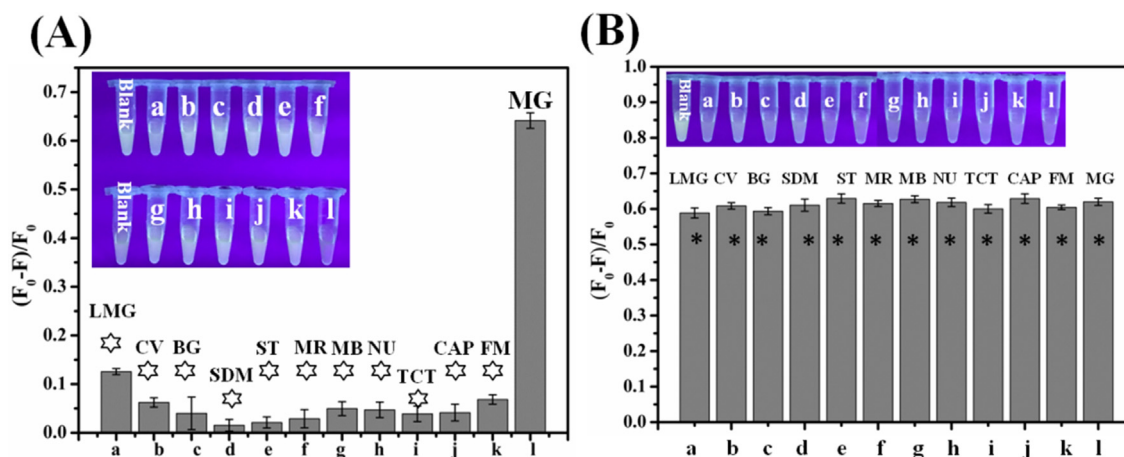


Fig. 6. Selectivity (A) and anti-interference (B) tests of the fluorescence method to different interferents. (Apt $0.3 \mu\text{mol L}^{-1}$, SGI $0.6 \times$ and MG $0.3 \mu\text{mol L}^{-1}$. Each of the concentrations of LMG, BG, CV, SDM, ST, MR, MB, NU, OTH, CAP and FM was set as $3 \mu\text{mol L}^{-1}$ ☆: significant difference ($p \leq 0.05$) compared with MG. *: no significant difference at $p > 0.05$. Insets: the photofluorography under 365 nm UV light. Error bars represented the standard deviations of three replicates.).

Table 2. Adding standard recoveries of MG detection in fish and water samples by fluorescence method and HPLC method.

Samples	Added ($\mu\text{g L}^{-1}$)	Fluorescence method			HPLC method		
		Found ($\mu\text{mol L}^{-1}$)	Recovery (%)	RSD (%)	Found ($\mu\text{mol L}^{-1}$)	Recovery (%)	RSD (%)
Sablefish (<i>Gadus morhua</i>)	0	Not detected	—	—	—	—	—
	0.05	0.048 ± 0.002	96.4	3.9	0.047 ± 0.002	93.5	3.2
	0.15	0.145 ± 0.007	96.7	4.4	0.142 ± 0.013	94.7	7.8
	0.3	0.273 ± 0.009	91.3	2.4	0.271 ± 0.007	89.1	3.2
Prawn (<i>Penaeus chinensis</i>)	0	Not detected	—	—	—	—	—
	0.05	0.053 ± 0.005	106.9	4.3	0.051 ± 0.002	103.2	3.1
	0.15	0.138 ± 0.009	91.5	6.4	0.136 ± 0.011	90.8	8.1
	0.3	0.289 ± 0.004	96.5	1.5	0.290 ± 0.013	96.7	4.7
Sea water (from Longzhou Pond in Jimei, Xiamen)	0	Not detected	—	—	—	—	—
	0.05	0.049 ± 0.002	97.7	4.2	0.044 ± 0.010	88.5	4.9
	0.15	0.136 ± 0.005	90.6	3.9	0.147 ± 0.008	93.3	5.4
	0.3	0.261 ± 0.012	87.1	3.5	0.268 ± 0.019	89.3	5.9

detect MG residues in fish samples with high accuracy and reliability.

4. Conclusions

The rapid and sensitive method for MG detection was realized based on the conformational changes of Apt and the fluorescence staining of SGI. The fluorescence quenching efficiency showed good linear relationship for MG concentrations in the range of $0.02\text{--}1.0 \mu\text{mol L}^{-1}$, the LOD of detection method was $0.61 \mu\text{g kg}^{-1}$. The method was successfully applied to the detection of fish samples and seawater. The detection can be completed within 40 min. The adding standard recoveries ranged from 87.1% to 106.9% with RSD of 3.5%–6.4%. The results were consistent with those of HPLC method. The results showed that the

established fluorescence method was sensitive, accurate, and convenient, and could be used to detect MG in fish samples.

Conflict of interest

The authors declare that they have no known competing financial interests or personal relationships that could have appeared to influence the work reported in this paper.

Acknowledgments

This study was supported by the National Natural Science Foundation of China (No. 21804050), the Fujian Provincial Fund Project (2018J01432), and the Xiamen Science and Technology Planning Project, China (3502Z20183031).

Appendix.

Aptamers:

KANA-Apt: 3-TGGGGGGTTGAGGCTAAGCC
 GA-5,
 CAP-Apt: 3-AC TTCAGTGAGTTGTCCCAC
 GGTCGGCGAGTCGGTGGTAG-5,
 SDM-Apt: 3-GAGGGCAACGAGTGTTTATA
 GA-5,
 OTA-Apt: 3-GATCGGGTGTGGGTGGCGTA
 AAGGGAGCATCGGACA-5,
 TCT-Apt: 3-CGTACGGAATTCGCTAGCCCC
 CGGCAGGCCACGGCTTGGGTGGTCC-
 CACTGCGCGTGGATCCGAGCTCCACGTG-5,
 Prope-1: 3-CTCAGATCTAACC-5,
 Prope-2: 3-CTCAGATCTAACCTTGTTA-5,
 Prope-3: 3- CTCAGATCTAACCTTGTTAAATT-
 GAGAAAAAA-5.

All of the aptamers supplied by Sangon Biotech Co., Ltd. (Shanghai, China) were diluted to $10 \mu\text{mol L}^{-1}$ with ddH₂O and stored at $-20 \text{ }^\circ\text{C}$ before use.

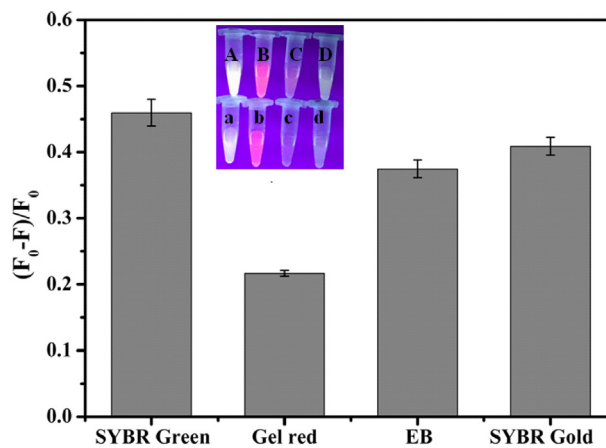


Fig. S1. Comparison of the fluorescence quenching efficiency $((F_0 - F)/F_0)$ with different fluorescent dyes. ($0.3 \mu\text{mol L}^{-1}$ Apt, $0.2 \mu\text{mol L}^{-1}$ MG, $0.6 \times$ SGI. Error bars represented the standard deviations of three replicates. Inset: the photofluorography of SGI (A), Gel red (B), EB (C), and SYBR Gold (D) in the absence of MG, while the lowercases represented those in the presence of MG).

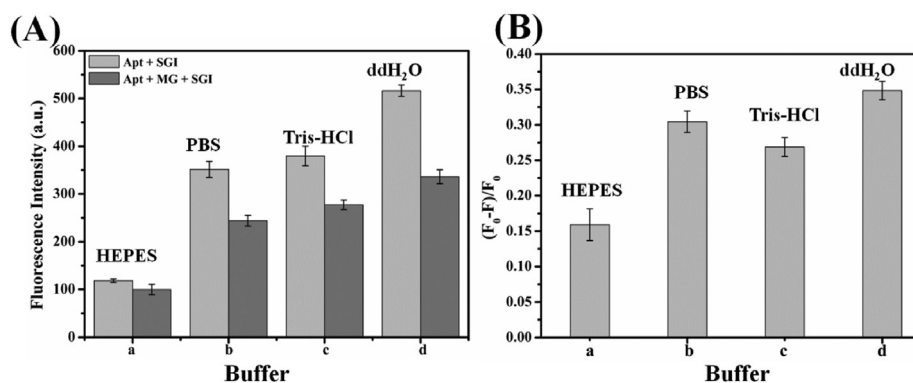


Fig. S2. Comparison of different buffers on the fluorescence intensity (A) and the fluorescence quenching efficiency $(F_0 - F)/F_0$ (B) in the detection solutions. (50 mmol L⁻¹ HEPES, pH 7.3; 20 mmol L⁻¹ PBS, pH 7.3; 20 mmol L⁻¹ Tris-HCl, pH 7.3. Concentrations: 0.3 $\mu\text{mol L}^{-1}$ Apt, 0.2 $\mu\text{mol L}^{-1}$ MG, 0.6 \times SGI. Error bars represented the standard deviations of three replicates.

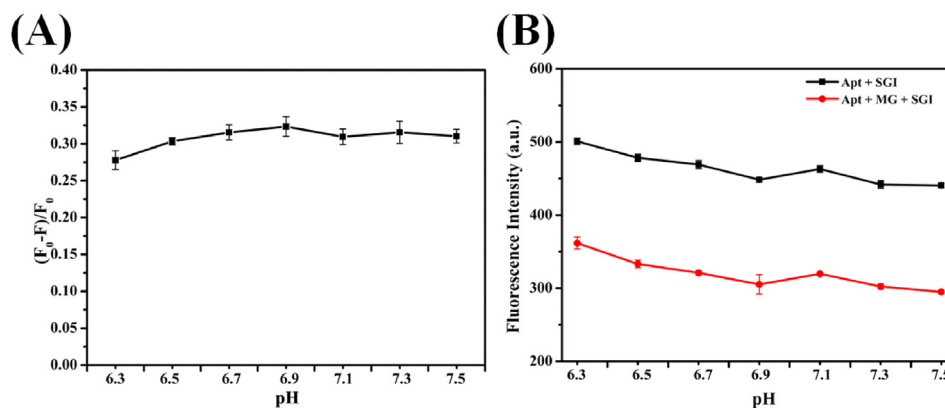


Fig. S3. Effect of pH values on $(F_0 - F)/F_0$ (A) and fluorescence (B). (0.3 $\mu\text{mol L}^{-1}$ Apt, 0.6 \times SGI, 0.2 $\mu\text{mol L}^{-1}$ MG. Error bars represented the standard deviations of three replicates).

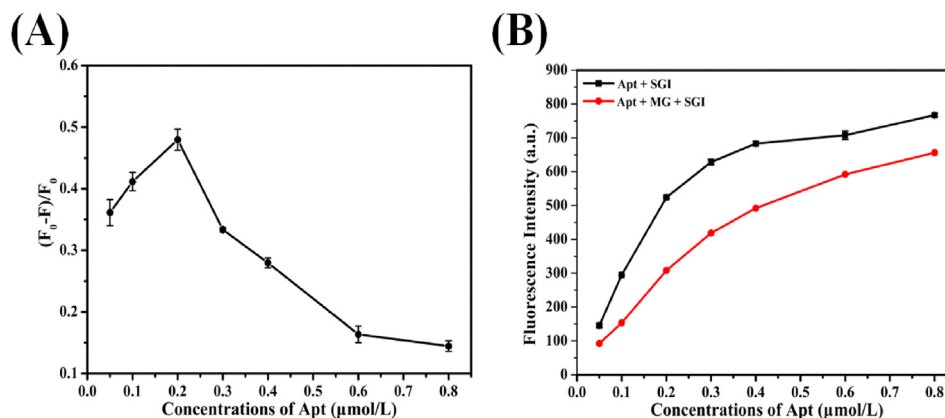


Fig. S4. Effect of the Apt concentrations on $(F_0 - F)/F_0$ (A) and fluorescence (B). (0.6 \times SGI, 0.2 $\mu\text{mol L}^{-1}$ MG. Error bars represented the standard deviations of three replicates).

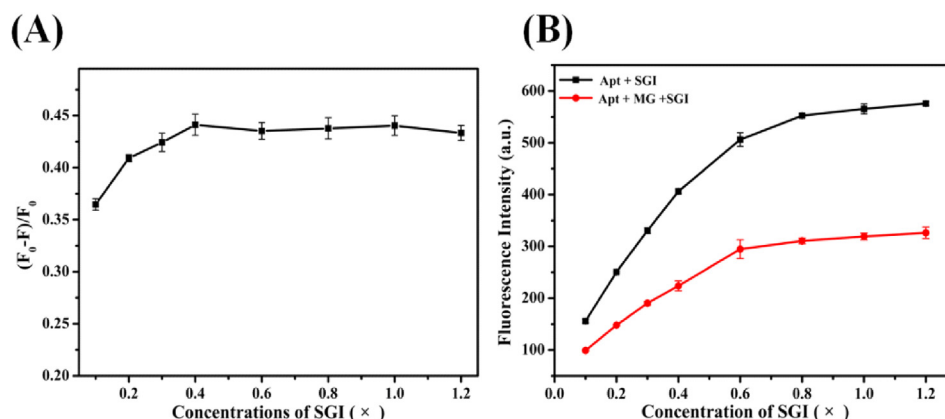


Fig. S5. Effect of SGI concentrations on $(F_0 - F)/F_0$ (A) and fluorescence (B). ($0.2 \mu\text{mol L}^{-1}$ Apt, $1.0 \mu\text{mol L}^{-1}$ MG. Error bars represented the standard deviations of three replicates).

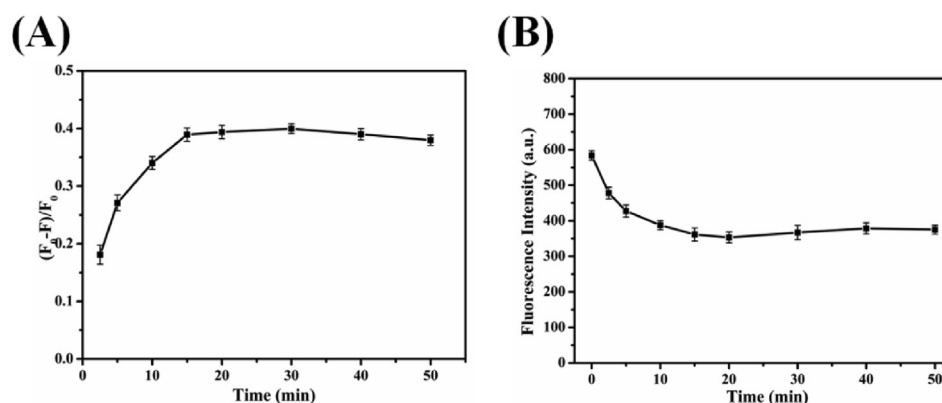


Fig. S6. Effect of binding time of MG to Apt on $(F_0 - F)/F_0$ (A) and fluorescence (B). ($0.2 \mu\text{mol L}^{-1}$ Apt, $0.6 \times$ SGI, $0.2 \mu\text{mol L}^{-1}$ MG. Error bars represented the standard deviations of three replicates).

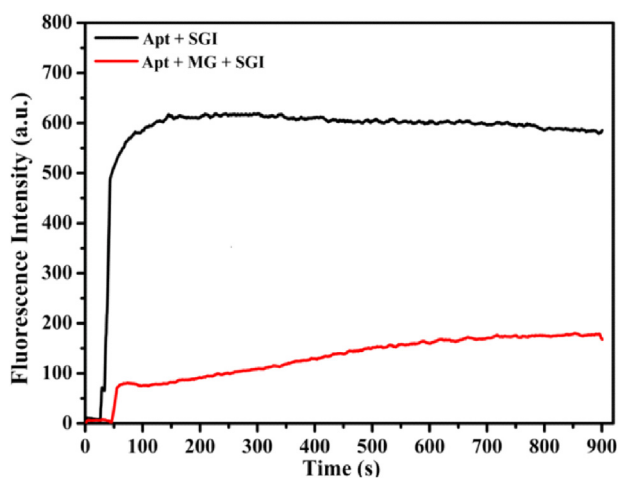


Fig. S7. Effect of incubation time after adding SGI on fluorescence. ($0.2 \mu\text{mol L}^{-1}$ Apt, $0.6 \times$ SGI, $0.2 \mu\text{mol L}^{-1}$ MG).

References

- [1] Patidar D, Goyal S. Adsorptive removal of malachite green dye from aqueous solution using a non carbon adsorbent: equilibrium, kinetics and thermodynamics. *J Adv Sci Res* 2021;1(2):19–23.
- [2] Das KC, Dhar SS. Rapid catalytic degradation of malachite green by MgFe_2O_4 nanoparticles in presence of H_2O_2 . *J Alloys Compd* 2020;828:154462.
- [3] Sasmal D, Banerjee S, Senapati S, Tripathy T. Effective removal of Th^{4+} , Pb^{2+} , Cd^{2+} , malachite green, methyl violet and methylene blue from their aqueous solution by amylopectin dialdehyde-Schiff base. *J Environ Chem Eng* 2020;8(3): 103741.
- [4] Brito SC, Bresolin JD, Sivieri K, Ferreira MD. Low-density polyethylene films incorporated with silver nanoparticles to promote antimicrobial efficiency in food packaging. *Food Sci Technol Int* 2020;26(4):353–66.
- [5] Vigneshwaran S, Sirajudheen P, Karthikeyan P, Meenakshi S. Fabrication of sulfur-doped biochar derived from tapioca peel waste with superior adsorption performance for the removal of Malachite green and Rhodamine B dyes. *Surface Interfac* 2021;23:100920.

- [6] Iglesias A, Nebot C, Vázquez BI, Coronel-Olivare C, Franco CM, Cepeda A. Monitoring the presence of 13 active compounds in surface water collected from rural areas in Northwestern Spain. *Int J Environ Res Publ Health* 2014; 11(5):5251–72.
- [7] Han S, Han WB, Chen J, Sun Y, Dai M, Zhao G. Bioremediation of malachite green by cyanobacterium *Synechococcus elongatus* PCC 7942 engineered with a triphenylmethane reductase gene. *Appl Microbiol Biotechnol* 2020;104(7):3193–204.
- [8] Singh R, Singh RK. Detection of malachite green in water using edge excited label free fluorescent probe NCQDs. *J Fluoresc* 2020;30(6):1281–5.
- [9] Souza ACP, Melo KM, de Azevedo LFC, Vilhena AOA, Nagamachi CY, Pieczarka JC. Lethal and sublethal exposure of *Hemichromis bimaculatus* (Gill, 1862) to malachite green and possible implications for ornamental fish. *Environ Sci Pollut Res* 2020;27(26):33215–25.
- [10] Teepoo S, Wongtongdee U, Phapugrangkul P. Development of qualitative and quantitative immunochromatographic strip test assay for rapid and simple detection of leucomalachite green residual in aquatic animals. *Food Chem* 2020; 320:126613.
- [11] Sinha R, Jindal R. Oxidative stress and toxicopathic branchial lesions in *Cyprinus carpio* exposed to malachite green. *Bull Environ Contam Toxicol* 2021;1–8.
- [12] Li T, Tian D, Zhu Z, Jin W, Wu S, Li H. The gut microbiota: a new perspective on the toxicity of malachite green (MG). *Appl Microbiol Biotechnol* 2019;103(23):9723–37.
- [13] Pipoyan D, Stepanyan S, Beglaryan M, Stepanyan S, Mantovani A. Health risk assessment of toxicologically relevant residues in emerging countries: a pilot study on Malachite Green residues in farmed freshwater fish of Armenia. *Food Chem Toxicol* 2020;143:111526.
- [14] Wei SC, Fan S, Lien CW, Unnikrishnan B, Chang HT. Graphene oxide membrane as an efficient extraction and ionization substrate for spray-mass spectrometric analysis of malachite green and its metabolite in fish samples. *Anal Chim Acta* 2018;1003:42–8.
- [15] Xie J, Peng T, Chen DD, Zhang QJ, Wang GM, Wang X, et al. Determination of malachite green, crystal violet and their leuco-metabolites in fish by HPLC-VIS detection after immunoaffinity column clean-up. *J Chromatogr B* 2013; 913–914:123–8.
- [16] Dong JX, Xu C, Wang H, Xiao ZL, Gee SJ, Li ZF, et al. Enhanced sensitive immunoassay: noncompetitive phage anti-immune complex assay for the determination of malachite green and leucomalachite green. *J Agric Food Chem* 2014;62(34):8752–8.
- [17] Asfaram A, Ghaedi M, Goudarzi A, Soyak M, Langroodi SM. Magnetic nanoparticle based dispersive micro-solid-phase extraction for the determination of malachite green in water samples: optimized experimental design. *New J Chem* 2015;39(12):9813–23.
- [18] Hakami AAH, Ahmed MA, Khan MA, Allothman Z, Rafatullah M, Islam MA, et al. Quantitative analysis of malachite green in environmental samples using liquid chromatography-mass spectrometry. *Water* 2021; 13(20):2864.
- [19] Ascari J, Drac S, Santos FA, Lima JA, Diniz MHG, Vargas EA. Validation of an LC-MS/MS method for malachite green (MG), leucomalachite green (LMG), crystal violet (CV) and leucocrystal violet (LCV) residues in fish and shrimp. *Food Addit Contam* 2012;29(4):602–8.
- [20] Hua Z, Yu T, Liu D, Xianyu Y. Recent advances in gold nanoparticles-based biosensors for food safety detection. *Biosens Bioelectron* 2021;179:113076.
- [21] Zhou JH, Rossi J. Aptamers as targeted therapeutics: current potential and challenges. *Nat Rev Drug Discov* 2017;16(3): 181–202.
- [22] Morita Y, Leslie M, Kameyama H, Kameyama H, Volk DE, Tanaka T. Aptamer therapeutics in cancer: current and future. *Cancers* 2018;10(3):80.
- [23] Moutsopoulos A, Broyles D, Dikici E, Daunert S, Deo SK. Molecular aptamer beacons and their applications in sensing, imaging, and diagnostics. *Small* 2019;15(35):1902248.
- [24] Pehlivan ZS, Torabfam M, Kurt H, Ow-Yang C, Hildebrands N, Yüce M. Aptamer and nanomaterial based FRET biosensors: a review on recent advances (2014–2019). *Microchim Acta* 2019;186(8):1–22.
- [25] Ștefan G, Hosu O, De Wael K, Lobo-Castañón MJ, Cristea C. Aptamers in biomedicine: selection strategies and recent advances. *Electrochim Acta* 2021;376:137994.
- [26] Bauer M, Strom M, Hammond DS, Shigdar S. Anything you can do, I can do better: can aptamers replace antibodies in clinical diagnostic applications? *Molecules* 2019;24(23):4377.
- [27] Ilgu M, Nilsen-Hamilton M. Aptamers in analytics. *Analyst* 2016;141(5):1551–68.
- [28] Malvano F, Pilloton R, Albanese D. Label-free impedimetric biosensors for the control of food safety—a review. *Int J Environ Anal Chem* 2020;100(4):468–91.
- [29] Jia J, Yan S, Lai XX, Xu YZ, Liu T, Xiang YH. Colorimetric aptasensor for detection of malachite green in fish sample based on RNA and gold nanoparticles. *Food Anal Methods* 2018;11(6):1668–76.
- [30] Deng PH, Feng JX, Wei YP, Xiao JY, Li JH, He QG. Fast and ultrasensitive trace malachite green detection in aquaculture and fisheries by using hexadecylpyridinium bromide modified electrochemical sensor. *J Food Compos Anal* 2021;102: 104003.
- [31] Chen X, Chen K, Du Z, Chu H, Zhu L, He X, et al. Fusion of binary split allosteric aptasensor for the ultra-sensitive and super-rapid detection of malachite green. *J Hazard Mater* 2022;425:127976.
- [32] Yoo YJ, Lee CH, Park SH, Lim YT. Nanoparticle-based delivery strategies of multifaceted immunomodulatory RNA for cancer immunotherapy. *J Contr Release* 2022;343:564–83.
- [33] Chen X, Li T, Tu X, Luo L. Label-free fluorescent aptasensor for thrombin detection based on exonuclease I assisted target recycling and SYBR Green I aided signal amplification. *Sens Actuators B* 2018;265:98–103.
- [34] Dragan A, Pavlovic R, McGivney J, Casas-Finet J, Bishop E, Strouse R, et al. SYBR Green I: fluorescence properties and interaction with DNA. *J Fluoresc* 2012;22(4):1189–99.
- [35] Wang H, Wang J, Sun N, Cheng H, Chen H, Pei R. Selection and characterization of malachite green aptamers for the development of light-up probes. *ChemistrySelect* 2016;1(8): 1571–4.
- [36] McKeague M, Velu R, Hill K, Bardóczy V, Mészáros T, DeRosa MC. Selection and characterization of a novel DNA aptamer for label-free fluorescence biosensing of ochratoxin A. *Toxins* 2014;6(8):2435–52.
- [37] Yang CY, Bie J, Zhang XM, Yan CY, Li HJ, Zhang MH, et al. A label-free aptasensor for the detection of tetracycline based on the luminescence of SYBR Green I. *Spectrochim Acta Part A* 2018;202:382–8.
- [38] Chang YM, Chen CKM, Hou MH. Conformational changes in DNA upon ligand binding monitored by circular dichroism. *Int J Mol Sci* 2012;13(3):3394–413.
- [39] Paramasivan S, Rujan I, Bolton PH. Circular dichroism of quadruplex DNAs: applications to structure, cation effects and ligand binding. *Methods* 2007;43(4):324–31.
- [40] Bahreyni A, Ramezani M, Alibolandi M, Hassanzadeh P, Abnous K, Taghdisi SM. High affinity of AS1411 toward copper; its application in a sensitive aptasensor for copper detection. *Anal Biochem* 2019;575:1–9.
- [41] O'Neil CS, Beach JL, Gruber TD. Thiazole orange as an everyday replacement for ethidium bromide and costly DNA dyes for electrophoresis. *Electrophoresis* 2018;39(12): 1474–7.
- [42] Cao YY, Wang XR, Bai HJ, Jia P, Zhao YJ, Liu YN, et al. Fluorescent detection of tetracycline in foods based on carbon dots derived from natural red beet pigment. *LWT* 2022: 113100.
- [43] Halme K, Lindfors E, Peltonen K. A confirmatory analysis of malachite green residues in rainbow trout with liquid

- chromatography-electrospray tandem mass spectrometry. *J Chromatogr B* 2007;845(1):74–9.
- [44] Xie J, Peng T, Chen DD, Zhang QJ, Wang GM, Wang X, et al. Determination of malachite green, crystal violet and their leuco-metabolites in fish by HPLC-VIS detection after immunoaffinity column clean-up. *J Chromatogr B* 2013;913–914:123–8.
- [45] Jiang Y, Chen L, Hu K, Yu W, Yang X, Lu L. Development of a fast ELISA for the specific detection of both leucomalachite green and malachite green. *J Ocean Univ China* 2015;14(2):340–4.
- [46] Chen XW, Nguyen TH, Gu LQ, Lin MS. Use of standing gold nanorods for detection of malachite green and crystal violet in fish by SERS. *J Food Sci* 2017;82(7):1640–6.
- [47] Ghasemi E, Kaykhahi M. Application of micro-cloud point extraction for spectrophotometric determination of malachite green, crystal violet and Rhodamine B in aqueous samples. *Spectrochim Acta Part A* 2016;164:93–7.
- [48] Wang QQ, Qin XF, Geng LP, Wang Y. Label-free electrochemical aptasensor for sensitive detection of malachite green based on Au nanoparticle/graphene quantum dots/tungsten disulfide nanocomposites. *Nanomaterials* 2019;9(2):229.
- [49] Shukla D, Pandey FP, Kumari P, Basu N, Tiwari MK, Lahiri J, et al. Label-free fluorometric detection of adulterant malachite green using carbon dots derived from the medicinal plant source *ocimum tenuiflorum*. *ChemistrySelect* 2019;4(17):4839–47.
- [50] Ju YJ, Li N, Liu SG, Han L, Xiao N, Luo HQ, et al. Ratiometric fluorescence method for malachite green detection based on dual-emission BSA-protected gold nanoclusters. *Sens Actuators B* 2018;275:244–50.
- [51] Zhao C, Hong CY, Lin ZZ, Chen XM, Huang ZY. Detection of malachite green using a colorimetric aptasensor based on the inhibition of the peroxidase-like activity of gold nanoparticles by cetyltrimethylammonium ions. *Microchim Acta* 2019;186(5):322.
- [52] Sczepanski JT, Joyce GF. Binding of a structured D-RNA molecule by an L-RNA aptamer. *J Am Chem Soc* 2013;135(36):13290–3.
- [53] Zhao C, Hong CY, Lin ZZ, Chen XM, Huang ZY. Detection of Malachite Green using a colorimetric aptasensor based on the inhibition of the peroxidase-like activity of gold nanoparticles by cetyltrimethylammonium ions. *Microchim Acta* 2019;186:322.
- [54] Chen XX, Lin ZZ, Hong CY, Yao QH, Huang ZY. A dichromatic label-free aptasensor for sulfadimethoxine detection in fish and water based on AuNPs color and fluorescent dyeing of double-stranded DNA with SYBR Green I. *Food Chem* 2020;309(30):125712.